

# The INTOA Experiment: A study of the ocean-atmosphere interactions under moderate to strong offshore winds and opposing swell conditions, in the Gulf of Tehuantepec, México

F. J. Ocampo-Torres,<sup>1</sup> H. García,<sup>1</sup> R. Durazo,<sup>2</sup> P. Osuna,<sup>1</sup> H. C. Graber<sup>3</sup>

**Abstract.** An air-sea interaction experiment (INTOA) took place from February to April 2005 in the Gulf of Tehuantepec, under the Programme for the Study of the Gulf of Tehuantepec (**PEGOT**, spanish acronym for Programa para el Estudio del Golfo de Tehuantepec). **PEGOT** is underway aiming for a better knowledge of the effect of strong and persistent offshore winds on coastal waters and their natural resources, as well as performing advanced modelling of the wave and surface current fields. One of the goals of the INTOA experiment was to improve our knowledge on air-sea interaction processes with particular emphasis on the effect of surface waves over momentum flux in the characteristic and unique conditions that occur when the strong *Tehuano* winds blow offshore against the Pacific Ocean long period swell. For the field campaign, an Air-Sea Interaction Spar (ASIS) buoy was deployed in the Gulf of Tehuantepec to measure surface waves and the momentum flux between the ocean and the atmosphere, in particular for offshore wind events under opposing swell conditions. High frequency radar systems (phase array type) were in operation in two coastal sites and 3 acoustic Doppler current profilers were deployed nearshore. Synthetic aperture radar images were also acquired as part of the remote sensing component of the experiment. The present paper provides the main results on the wave and wind fields mainly regarding the direct calculation of the momentum flux and the drag coefficient, and gives an overview of the INTOA experiment.

## 1. Introduction

Momentum exchange between the atmosphere and ocean together with fluxes of heat and moisture, play a fundamental role on weather, and climate and its variability, over a wide range of time and space scales. A good number of experiments and field campaigns have been carried out to better understand the fundamental processes related to air-sea interaction and the underlying physics of various phenomena influencing directly the atmospheric boundary layer or the ocean mixed layer: FETCH 2 [2], SOWEX 4 [4], FASTEX 6 [6], just to mention some of the most recent ones. All those experiments have yielded important contributions to the understanding of air-sea transfer processes, however, there are still open questions. In particular, the influence of the sea state and underlying swell on the air-sea interaction requires further study to adequately understand fundamental processes.

Knowledge on how momentum flux or wind stress vary with environmental parameters is of increasing importance, especially to properly modeling air-sea interactions for ocean current and wave prediction. The most important parameters are mainly associated with the ocean surface waves, therefore the wave field is a key factor in

---

<sup>1</sup>Departamento de Oceanografía Física, División de Oceanología, CICESE, Ensenada BC, México.

<sup>2</sup>Facultad de Ciencias Marinas, Universidad Autónoma de Baja California, Ensenada, BC, México.

<sup>3</sup>Rosenstiel School of Marine and Atmospheric Science, University of Miami, Miami, Florida, USA.

this respect.

In this context, the INTOA experiment was organized and carried out in the Gulf of Tehuantepec, where very distinctive processes make it a unique place since moderate to strong winds show persistent direction due South (*Tehuano* events), while long period swell arrives to the study region traveling practically Northwards.

The *Tehuano* events are stronger and more common during the winter, and the area can easily be considered as a natural laboratory where specific studies dealing with the interaction of locally generated wind-sea and opposing swell are very appealing. The analysis of the wave field evolution under fetch limited conditions is also of great interest in the study region.

The INTOA experiment is one component of the PEGoT programme. PEGoT is underway aiming for a better knowledge of the effect of strong and persistent offshore winds on coastal waters and their natural resources, as well as to perform advanced modeling of the wave and surface current fields. Under the PEGoT programme various research projects are being carried out, dealing with determination of the influence of *Tehuano* events on the surface circulation as being inferred through high frequency radar systems, as well as analyzing the genesis of oceanic eddies and their interaction with larger scale circulation in the Tropical Pacific Mexican waters.

The INTOA experiment main objectives are defined as: 1) to improve our knowledge on air-sea interaction processes with particular emphasis on the effect of surface waves over momentum flux in the characteristic local conditions that occur in the Gulf of Tehuantepec, when the strong *Tehuano* winds blow offshore against the Pacific Ocean long period swell arriving from the South; 2) to describe momentum flux dependence on environmental conditions, such as the sea state, ocean swell, wind field and ocean surface currents; 3) to determine the evolution of wave field in coastal waters and under a combination of locally generated wind-sea and swell in the opposite direction, with emphasis on the attenuation of swell; 4) to characterize the influence of *Tehuano* events as forcing mechanism on surface currents; and 5) to test wave retrieval algorithms being applied to remote sensing information as obtained from synthetic aperture and high frequency radar systems.

The purpose of this paper is very much linked to main objectives 1) and 2) above, as the description of the wave field evolution and wind conditions, specifically regarding the direct calculation of momentum fluxes and the drag coefficient. We also provide some background and the goals of PEGoT, and the main objectives of the air-sea interaction component, the set up for the INTOA experiment and field campaign, and an overview of the dominant oceanic and atmospheric conditions.

Although we briefly show preliminary results on the remote sensing component of the experiment, those other aspects such as the high frequency radar (HF WERA) systems detailed description and results, and further analysis of advanced synthetic aperture radar (ASAR) images to provide quantitative information on wind fields and the spatial evolution of swell, are to be left out of the scope of the present paper and they will be considered in another contribution.

In the following section a brief description of the INTOA Experiment is provided. A section with the main results follows, explaining the overall mean conditions, wind and waves characteristics encountered, and some relevant aspects of the momentum flux and the drag coefficient as they are calculated directly from the measurements. Final remarks are given in the last section.

## 2. Field campaign

The INTOA experiment measuring campaign was carried out from February to April 2005 in the Gulf of Tehuantepec. Momentum flux, wave field, and other related atmospheric and oceanic variables were measured directly and simultaneously from a moored Air-Sea Interaction Spar (ASIS) buoy (see Figure 2). The location was selected to monitor air-sea interaction variables under fetch limited conditions during Tehuano events. The ASIS buoy is a stable platform especially designed for air-sea interaction studies, therefore it causes very low distortion of surface and wind flow 8 [10], it was attached to a tether buoy by a surface floating line of about 40 m long. Our ASIS buoy was deployed from the DR06 Bahía Tepoca Dredge Vessel (see Figure 3) from the Mexican Navy (Secretaría de Marina-Armada de México) and moored from 22 February to 24 April 2005 in the central part of the Gulf of Tehuantepec at 16°N, 95°W, approximately 22 km offshore at a 60 m depth location (Figure 1).

A list of the sensors included in the ASIS buoy and some of their characteristics are detailed in Table 1. The three turbulent components of the wind velocity were recorded with a sonic anemometer sampling at 20 Hz. Sea surface elevation was also sampled at 20 Hz by an array of 6 wave gauges continuously measuring capacitance. The buoy motion was detected and recorded at 20 Hz through the measurements of three linear accelerometers, a clinometer and a compass, providing the 6 components of motion of the buoy. Air temperature and humidity were sampled at 1 Hz, as well as atmospheric pressure. Sub-surface water temperature was measured every 5 s at the ASIS buoy while sub-surface current measurements every 10 min were obtained below the tether buoy. Recording the buoy motion is crucial in order to correct all other measurements and refer them to a proper coordinate system following available algorithms according to 10 [10], 12 [10], and 14 [10]. Data acquired during 30 min runs were considered to calculate the momentum flux through the eddy correlation method, directional wave spectra and averages or other variables reported herein, such as significant wave height, mean wave direction, mean wind speed and direction, etc. These measurements represent the first time a platform of this type is deployed successfully in Latinamerican waters.

Directional wave measurements and the current profile were acquired with ADCPs (Nortek, Aquadopp) deployed nearshore at three locations where water depth was about 20 m: 1) Espigon station at 16° 8.74' N 95° 12.13' W, 2) Castillo station at 16° 5.3' N 95° 15.9' W, and 3) Chipehua station at 16° 1.89' N 95° 21.39' W. Surface elevation and the three velocity components due to the wave motion were measured at a rate of 1 Hz during 1024 s every hour (every 1.5 hours for Chipehua Station), while current measurements for the vertical profile were sampled every 20 min at 1.0 m cells within the water column (average during 90 s). Surface wave directional spectra is then obtained every hour through standard MLM routines (16 [10]), while the current profile was obtained every 20 min at each of the three locations.

Additionally, two sites with high frequency radar systems (Wellen Radar, WERA) were in operation for the field campaign period, in order to retrieve surface current and wave fields. WERA stations were located at 16° 4.24' N 95° 21.76' W (Cangrejo, CAN) and 16° 12.94' N 94° 51.16' W (Santa Maria del Mar, STM). These phase array high frequency radar systems operated at 16.3 MHz with a typical coverage range of 100 km. Surface current and

wave fields can be retrieved every hour with a spatial resolution of approximately 1 km by 1 km. Complementing the remote sensing component of the experiment, some images of the ocean surface were also acquired through the Advanced Synthetic Aperture Radar (ASAR) onboard the European satellite ENVISAT. Sets of four single look complex images were acquired on February 26 at 04:20; March 02 at 16:20, and March 18 at 16:17, although in Fig. 1 we only show the frames for those images closer to the coast of the first two dates.

### 3. Results

#### 3.1. Overall wind conditions

Prevailing wind conditions during our field campaign were typical for the Gulf of Tehuantepec winter season. At least eight Tehuano events were present and maximum wind speed (average over 30 min) was detected between  $10\text{ms}^{-1}$  and  $19\text{ms}^{-1}$  (see Figure 4). Wind direction during these events is persistently to the South, while it varies between events when wind speeds are even lower than  $5\text{ms}^{-1}$ . In some cases moderate wind blowing towards the North was observed (day 58).

In general terms, total duration of Tehuano events detected varied from about 20h to 140h. The onset time observed was between 5h and 19h, although for most cases just about 6h were required to reach maximum wind speed. A characteristic sudden drop in wind speed in the middle of the event was observed in at least four of those events detected, showing wind speed as low as  $1\text{ms}^{-1}$ . This relaxation in wind speed is however, still an open question. Some characteristics of these events, including start date and time, are given in Table 2.

The frequency distribution of wind speed during the INTOA experiment is shown in Figure 5. Tehuano event speed distribution is also shown as rather wide compared with the total distribution. Furthermore, two relative maxima can be depicted, at low and high speeds (bimodal distribution). For the period of our measurements the frequency distribution for the full amount of wind speed data resembles a Rayleigh distribution with  $6\text{ms}^{-1}$  as the most frequent speed.

In Figure 6 the frequency distribution of wind directions is shown. During Tehuano events direction is practically concentrated towards  $190^\circ \pm 20^\circ$ . The full distribution shows two maxima, one corresponding with Tehuano events and the other one (as secondary maximum) with wind blowing to the North.

#### 3.2. Wave field characteristics

The wave field in the Gulf of Tehuantepec can be described by the presence of a complex sea state, ie. typically a combination of wind-sea and swell, where swell can be regarded as one or more systems. Furthermore, swell is practically present all year round. Whenever there is a *Tehuano* event, swell is practically opposing the wind direction, otherwise there might be swell along wind, with rather low to moderate wind speeds though.

Locally generated waves during Tehuano events were observed with significant wave height as high as 2.5m as measured by the ASIS buoy, approximately 20 km offshore. The same winds however, are known to generate higher waves further offshore. The presence of swell over the whole measuring period is very characteristic. Swell significant wave height varied from somewhat less than 0.5m to about 1.5m, as detected by the ADCPs nearshore (See Fig. 4).

In the Gulf of Tehuantepec we typically encounter an interesting combination of wind and waves, with charac-

teristics such as: 1) Offshore wind (moderate to strong) and opposing swell (low swell or high swell), 2) Other wind conditions (rather low wind) might allow swell present along wind, and 3) Presence of swell as one or more systems.

We focus this analysis to the wave field evolution for complex sea states when there is locally generated waves being forced by offshore winds and swell approaching the region in opposite direction. Swell conditions present are classified as low and high significant wave heights. We refer to low significant wave conditions when  $H_s$  is approximately 0.5m as average, while high significant wave conditions when  $H_s$  vary from 1.0 m to 1.5 m, approximately.

Time series of wave spectra as a function of frequency can be seen in Figure 7. For the case of wave spectra as obtained from the ADCP measurements nearshore (Figure 7 a), the time evolution of the wave field shows essentially the swell signal. Arrival of shorter swell as time goes by can be readily seen, showing the classical dispersion process when waves propagate away from the source (distant storms). The presence of one or more (sometimes even three) swell systems at a particular time is also depicted. Practically most of the swell energy is encountered between 0.05 Hz and 0.09 Hz frequency bands. Regarding the results from the ASIS buoy measurements (Figure 7 b)), spectral energy density in the high frequency (typically for  $f > 0.2$  Hz) region is observed, specially when associated to the presence of strong Tehuano events. Relatively low to moderate spectral energy events are also observed with intermediate frequencies ( $0.10\text{Hz} > f > 0.15\text{Hz}$ ), between low-frequency long swell and high-frequency short locally-generated (associated with Tehuano events) wind-waves, which can be related to minor storms relatively closer than those generating the strong swell. Ocean swell arrival and its variation as a function of time is also shown at frequencies somewhat around 0.1 Hz and lower.

An example of directional spectrum obtained from the ASIS buoy measurements is shown in Figure 8, for 01 March 2005 at 04:23 GMT (dd=60.1826). For this particular case a Tehuano event was on, therefore locally generated waves are readily apparent in the relatively high frequency region within the spectrum. The wind blowing offshore (note the arrow in the polar plot) is over  $15 \text{ ms}^{-1}$ .

The presence of more than one wave system was rather common during the experiment. In Figure 9 an example of directional wave spectrum is shown when three wave systems were depicted. This particular case is close in time to one of the ASAR image acquisition during the experiment.

### 3.3. Presence of swell

An example of the swell directional spectrum retrieved from the ADCP at Chipehua Station is shown in Figure 10. Waves were recorded at about 40 min after acquisition time for one of the ASAR images obtained. A well defined swell system is readily apparent showing main wave traveling direction between North and  $-30^\circ$ . Wind speed is rather low, about  $2 \text{ ms}^{-1}$  as shown by arrow from the center (recorded by ASIS buoy).

Analysis of swell propagation and evolution can also be performed through the information retrieved from ASAR images. In Fig. 11 an example of such an image is provided (See Fig. 1 for frame location and orientation as reference). ASAR images were acquired by the European satellite ENVISAT over the study region. This particular one is from February 26, 2005, where internal wave

packets can also be observed. A set of 5 sub-images (512 by 512 pixels each) were extracted from the image at locations given in Fig. 1 in the neighborhood of the ASIS buoy, to estimate the directional wave spectra shown in Fig. 12 to 16. Two swell systems appear to propagate towards North and towards  $-20^\circ$  relative to North, respectively. The wave systems main wavelength vary from 300m to about 180m, while overall estimate of significant wave height reveals a consistent and gentle increase (from 0.60m to 0.80m) as the swell propagates Northwards.

### 3.4. Momentum flux and the drag coefficient

From wind velocity components measured by the sonic anemometer onboard the ASIS buoy, the wind stress ( $\boldsymbol{\tau}$ ) can be directly calculated through the eddy correlation method as

$$\boldsymbol{\tau} = -\rho (\overline{u'w'\hat{i}} + \overline{v'w'\hat{j}}), \quad (1)$$

where  $u'$ ,  $v'$ , and  $w'$  are the turbulent velocity components,  $\rho$  is the air density and the overbar represents time averaging over 30 minutes. Wind stress is typically expressed in terms of the drag coefficient  $C_D$  by

$$\boldsymbol{\tau} = -\rho C_D U_z^2. \quad (2)$$

To avoid dependence of  $C_D$  on measuring height and atmospheric stability,  $C_D$  was computed for neutral conditions at the 10 meters standard height.

Wind speed was converted to neutral conditions value using the flux profile relation (18 [18])

$$U_{zN} = U_z + (u_*/\kappa)\psi_u(z/L) \quad (3)$$

where  $\kappa$  is the von Kármán constant,  $\psi_u$  represents the nondimensional gradient suggested by 18 [18], and  $L$  is the Monin-Obukhov length scale.

Wind speed at standard 10 m height was then calculated assuming a logarithmic wind profile

$$U_{10N} = U_{zN} + \frac{u_*}{\kappa} \log \frac{10}{z} \quad (4)$$

and the drag coefficient directly determined through 2.

The neutral drag coefficient at 10 m height ( $C_{D_{10N}}$ ) is plotted as a function of wind speed ( $U_{10N}$ ) in Figure 17. Single values of  $C_{D_{10N}}$  for each 30 minutes are represented by dots, diamonds are the average of  $C_{D_{10N}}$  within wind speed bins of  $1 \text{ ms}^{-1}$ , and error bars are one standard deviation of the variation of  $C_{D_{10N}}$  within each wind speed bin. For visual purposes all data points from the first bin (mean  $C_{D_{10N}} = 9.7 \times 10^{-3} \pm 6.9 \times 10^{-3}$ ) and 4 data points from the second bin were excluded from the graph. It can be seen that the drag coefficient tends to decrease with wind speed from low wind up to  $7 \text{ ms}^{-1}$  whereas for higher winds there is a linear increase and reduced scatter. The best fit for  $C_{D_{10N}}$  as a function of wind speed is:

$$C_{D_{10N}} = 1 \times 10^{-3} \begin{cases} 1 + 2.7U_{10N}^{-1} + 4.1U_{10N}^{-2} & U_{10N} < 7 \text{ ms}^{-1} \\ 0.73 + 0.083U_{10N} & U_{10N} > 7 \text{ ms}^{-1} \end{cases} \quad (5)$$

Observed  $C_{D_{10N}}$  values are moderate and consistently higher than those reproduced from commonly used rela-

tionships. In particular at low winds, no constant value was found in contrast to what has been earlier reported 20 [12]. The high drag coefficient values observed during low wind conditions are probably caused by the presence of swell as previously reported by 22 [24] for similar conditions of offshore winds in the Gulf of Mexico.

On the other hand, during moderate to high wind conditions ( $U_{10} > 7\text{ms}^{-1}$ ) almost all data, around 90%, correspond to northerly winds, i.e. offshore winds. Under these conditions at the fixed fetch of the buoy (22 km) wind generated waves are underdeveloped and wind seas became younger with increasing wind speed. Using a carefully selected set of data from several field experiments, it has been found (12 [12]), that for wind seas the sea surface roughness,  $z_0$ , increases with increasing wave age, defined as the ratio between the friction velocity and the phase speed of the wind sea peak frequency ( $u_*/C_p$ ). Under neutral conditions there is a unique relationship between the surface roughness and the drag coefficient

$$C_{D_{zN}} = \kappa^2 [\log(z/z_0)]^{-2} \quad (6)$$

hence is indistinctly to discuss in terms of  $z_0$  or  $C_D$ .

In figure 17 dotted lines represent the  $C_{D_{10N}}$  associated with the indicated wave age constant values, according to 12 [12] relationship. It seems that the observed  $C_{D_{10N}}$  for moderate to high wind conditions might be better represented by a relatively constant wave age  $u_*/C_p \sim 0.08$ , although under those conditions in reality the wind sea wave age increased linearly with wind speed and ranked, in average, from 0.05 at  $7\text{ms}^{-1}$  to 0.125 at  $20\text{ms}^{-1}$ . Corresponding values of  $C_{D_{10N}}$  for observed wave ages using 12 [12] pure wind seas formula are higher than the observed ones (not shown). It is worth to mention that the presence of swell can mask the relationship between wave age and surface roughness 24 [24]. Swell is present practically all over the study period, then 24 [24] relationship is used here only as a reference of what would be expected in the absence of swell, i.e. in pure wind sea conditions. We advance the hypothesis that the presence of swell, somehow, reduces the wind sea roughness, hence the  $C_{D_{10N}}$ . Observed drag coefficient in moderate to high wind conditions will correspond to  $C_{D_{10N}}$  associated with young waves that do not reach an hypothetical pure wind sea roughness value due to the influence from the background swell. A complete description of this matter however, escapes from the purposes of this manuscript and it is suggested to be dealt with in a further analysis and report it elsewhere.

## 4. Conclusions

The most important characteristics and overview of the INTOA Experiment have been presented here. Although it is clear that one single experiment is not enough to solve all still open questions, the initial objectives of the INTOA Experiment have been achieved.

**Acknowledgments.** The present work has been supported by CONACYT (62520, DIROCIOA), CICESE's Research Program for Wave Studies and UCMexUS-CONACYT (Collaborative Project Grant), while the INTOA experiment field campaign was supported by CONACYT (SEP-2003-C02-44718). We thank all the technical personnel who contributed to the success of the experiment, particularly Joe Gabrielle, Mike Rebozo, Neil Williams and Sergio Ramos, and the officers and crew of DR06 Bahía Tepoca. We are in debt to Pierre Flament for his assistance and contribution to build up the two radar sites for up to 16 channels each. BOOST Technologies allowed us to use their software to retrieve the wave spectrum from ASAR images. Special thanks to Julieta

Castro, Lina Zúñiga, Lupita Pacheco, and Mónica Sánchez for scientific activities coordination, logistic and administrative support. The final part of this work was developed during a sabbatical leave by FJO-T at ISMAR in Venice, with support from ICTP-TRIL Program, CONACYT (Programa de Estancias en el Extranjero) and CICESE. FJO-T would like to express his gratitude to Luigi Cavaleri and ISMAR staff for their support and hospitality.

## References

- D. Hauser, H. Branger, S. Bouffies-Cloch e, S. Despiau, W. M. Drennan, H. Dupuis, P. Durand, X. Durrieu de Madron, C. Estournel, L. Eymard, C. Flamant, H. C. Graber, C. Gu erin, K. Kahma, G. Lachaud, J.-M. Lef evre, J. Pelon, H. Petterson, B. Pignatelli, P. Queffelec, D. Tailliez, J. Tournaire, and A. Weill. The fetch experiment: An overview. *J. Geophys. Res.*, 108(C3):FET 1 (1–15), 2003.
- M. L. Banner, E. J. Wei Chen, E. J. Walsh, J. B. Jensen, C. Sunhee Lee, and C. Fandry. The southern ocean waves experiment, part 1, overview and mean results. *J. Phys. Oceanogr.*, 29(9):2130–2145, 1999.
- L. Eymard, G. Caniaux, H. Dupuis, L. Prieur, H. Giordani, R. Troade, P. Bessemoulin, G. Lachaud, G. Bouhours, D. Bourras, C. Gurin, P. Le Borgne, A. Brisson, and A. Marsouin. Surface fluxes in the north atlantic during catch/fastex. *Q. J. R. Meteorol. Soc.*, 125(561):3565–3599, 1999.
- M. A. Donelan, W. M. Drennan, J. C. V. Leer, H. C. Graber, E. A. Terray and D. B. Peters. Asis-a new air-sea interaction spar buoy: Design and performance at sea. *J. Atmos. Oceanic Technol.*, 17(5):708–720, 2000.
- K. K. Kahma, W. M. Drennan and M. A. Donelan. On momentum flux and velocity spectra over waves. *Boundary-Layer Meteorol.*, 92(nn):489–513, 1999.
- W. M. Drennan, H. C. Graber, D. Hauser, and C. Quentin. On the wave age dependence of wind stress over pure wind seas. *J. Geophys. Res.*, 108(C3):FET 10 (1–13), 2003.
- F. Ancil, M. A. Donelan, W. M. Drennan, and H. C. Graber. Eddy-correlation measurements of air-sea fluxes from a discuss buoy. *J. Atmos. Oceanic Technol.*, 11(4):1144–1150, 1994.
- W. M. Drennan, M. A. Donelan, N. Madsen, K. B. Katsaros, E. A. Terray, and C. N. Flagg. Directional wave spectra from a swath ship at sea. *J. Atmos. Oceanic Technol.*, 11(4):1109–1116, 1994.
- M. A. Donelan. Air-sea interaction. In B. Le M ehaut e and D. M. Hanes, editors, *The Sea Ocean Engineering Science*, volume 1, pages 239–292, 1990.
- W. G. Large and S. Pond. Open ocean momentum flux measurements in moderate to strong winds. *J. Phys. Oceanogr.*, 11:324–336, 1981.
- J. Pan, D. W. Wang, and P. A. Hwang. A study of wave effects on wind stress over the ocean in a fetch-limited case. *J. Geophys. Res.*, 110(C02020):doi:10.1029/2003JC002258, 2005.
- W. M. Drennan, P. K. Taylor, and M. J. Yelland. Parameterizing the sea surface roughness. *J. Phys. Oceanogr.*, 35(5):835–848, 2005.
- S. D. Smith. Wind stress and heat flux over the ocean in gale force winds. *J. Phys. Oceanogr.*, 10:709–729, 1980.

---

F. J. Ocampo-Torres, Departamento de Oceanograf a F isica, Divisi on de Oceanolog a, CICESE, Km 107 Carretera Tijuana-Ensenada, Ensenada BC, 22860, M exico. (ocampo@cicese.mx)

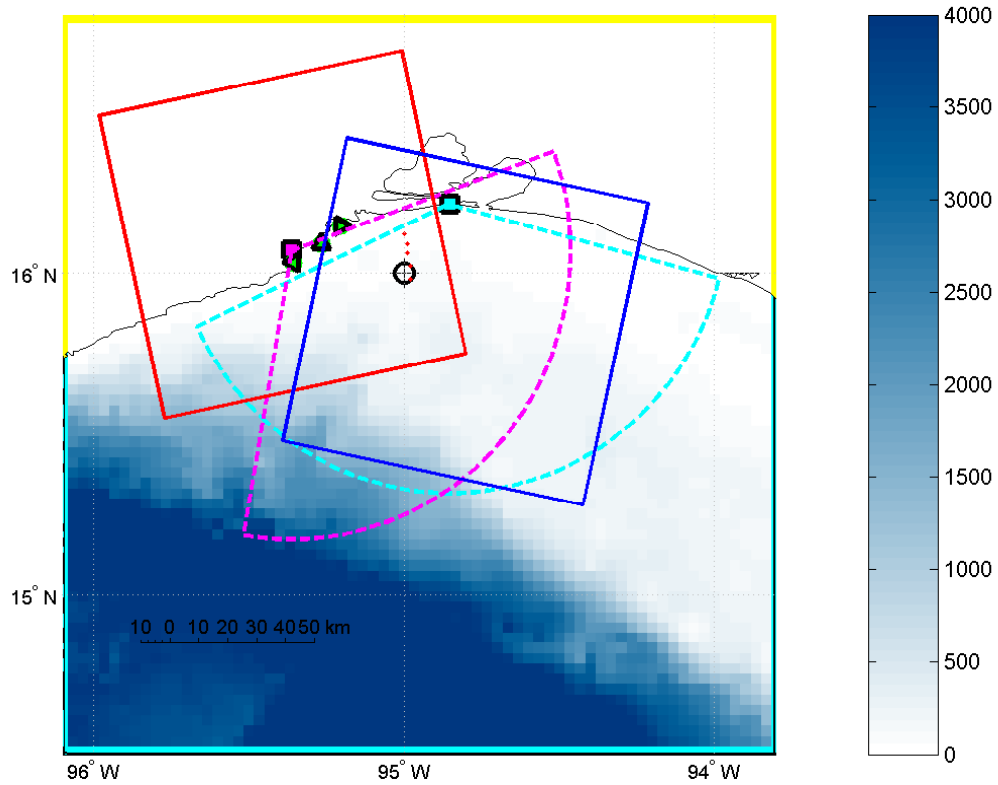


**Figure 1.** Map of the Gulf of Tehuantepec study area with color-coded bathymetry (depth in m). Frames correspond to two ASAR images acquired by ENVISAT on February 26 (Red frame) and March 2 (Blue frame). Mooring location for the ASIS buoy is also shown (circle with plus sign). Central position for five sub-scenes extracted from Feb-26 ASAR image to retrieve wave information and spectral estimates are shown (red dots) in the vicinity of the ASIS buoy location. HF radar WERA system sites (Squares filled with cyan and magenta) and coverage (Santa Mara del Mar STM: cyan; Cangrejo CAN: magenta). Location for nearshore deployed Nortek ADCPs (triangles filled with green) are for Espigon station (triangle pointing East), Castillo station (triangle pointing North), and Chipehua station (triangle pointing Westward).

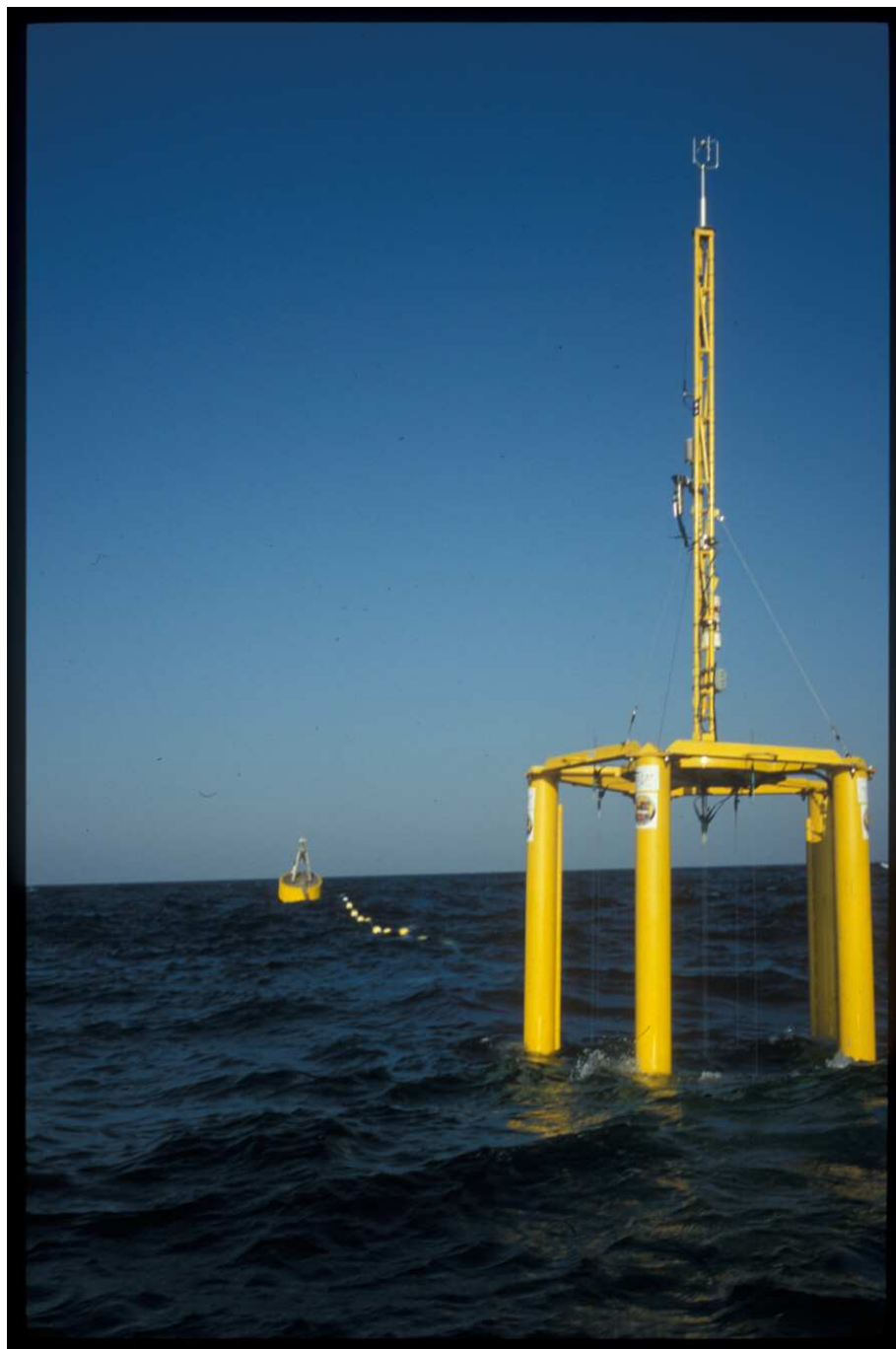


**Figure 2.** ASIS buoy in the Gulf of Tehuantepec during the INTOA experiment in 2005 attached to a tether buoy (in the back) by a line with floats.



**Figure 3.** Picture of the ASIS bouy in the Gulf of Tehuantepec during the INTOA experiment in 2005 and Bahía Tepoca DR06 Vessel.

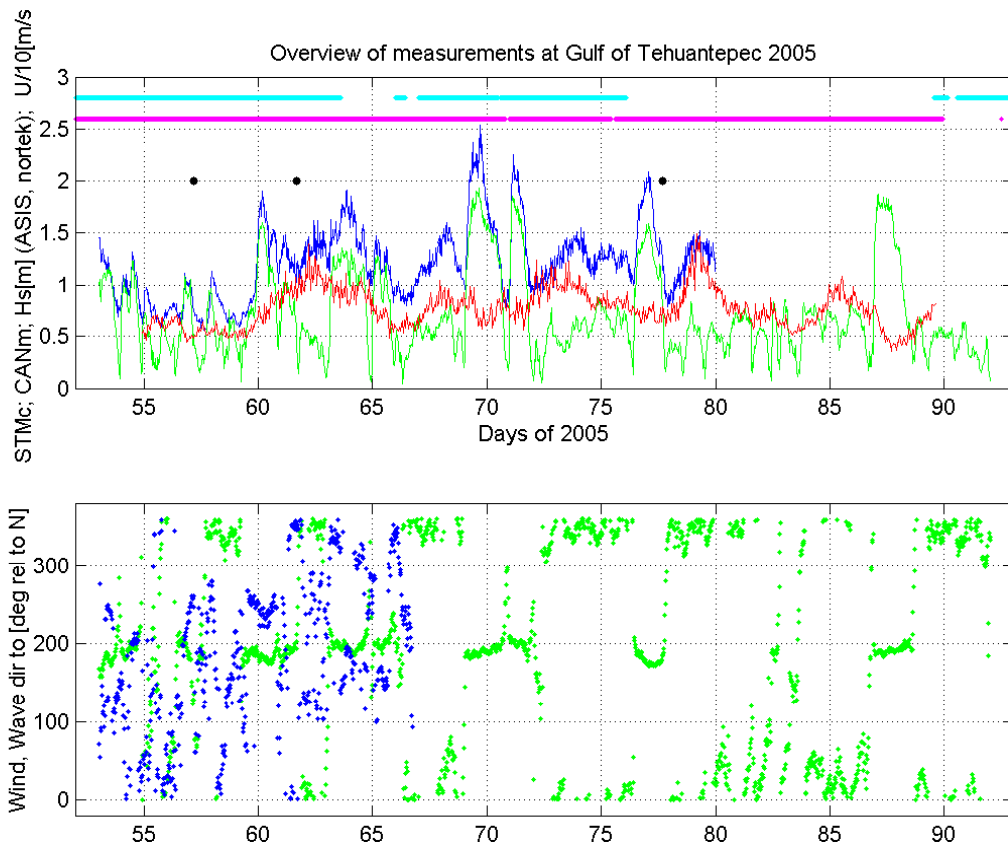


**Figure 4.** Overall mean conditions and overview of measurements in the Gulf of Tehuantepec during the INTOA experiment. Top panel: Horizontal lines indicate the period of time when the high frequency radar systems (WERA) were in operation (cyan: STM; magenta: CAN); Acquisition time for three sets of ASAR images are shown (black dots); Wind speed ( $\text{ms}^{-1}$ ) is scaled by a factor of 0.10 (green) and significant wave height is given in m (blue) as measured by the ASIS buoy, while significant wave height measured by an ADCP nearshore (red) is also shown. Bottom panel: Wind and mean wave direction (green and blue dots, respectively) are shown in degrees measured clockwise from North (oceanographic convention).

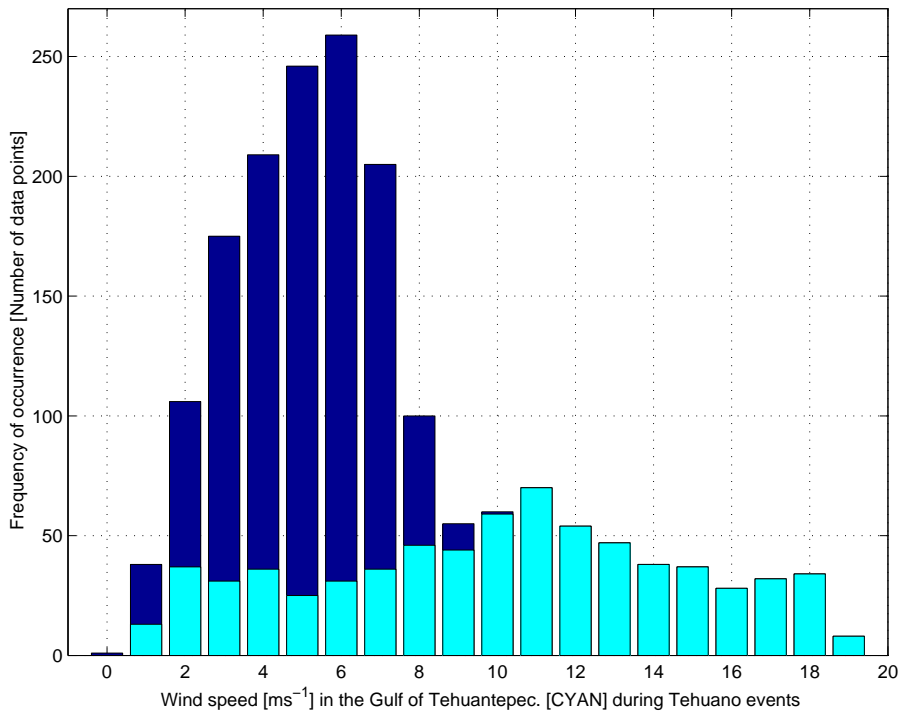


**Figure 5.** Frequency of occurrence distribution of wind speed during the INTOA experiment. Wind speed distribution for exclusively Tehuano events is depicted (Cyan bars).

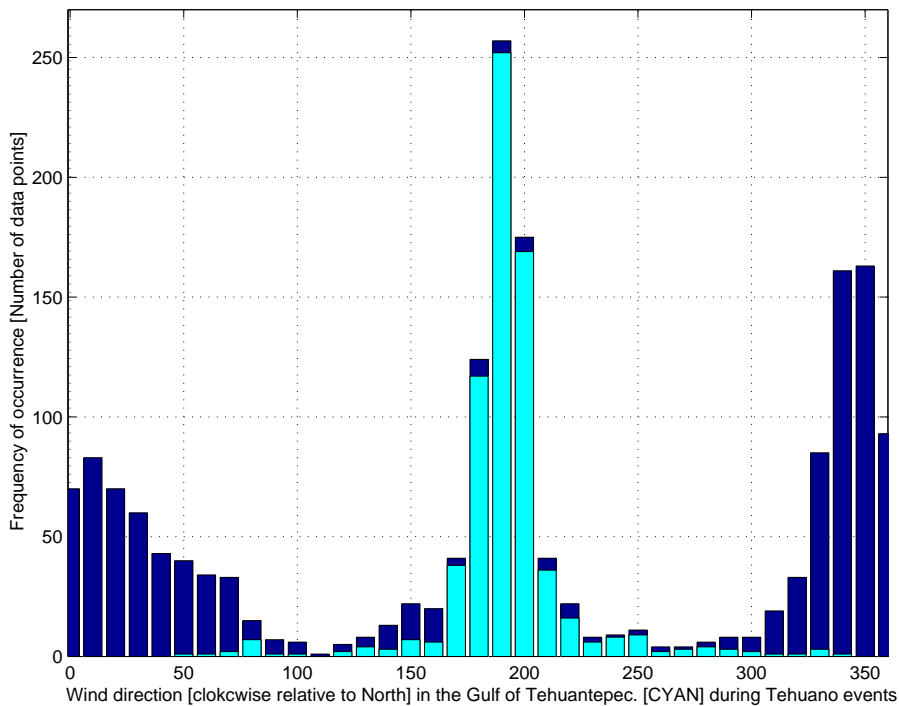


**Figure 6.** Frequency of occurrence distribution of wind direction during the INTOA experiment. Wind direction distribution for exclusively Tehuano events is depicted (Cyan bars).

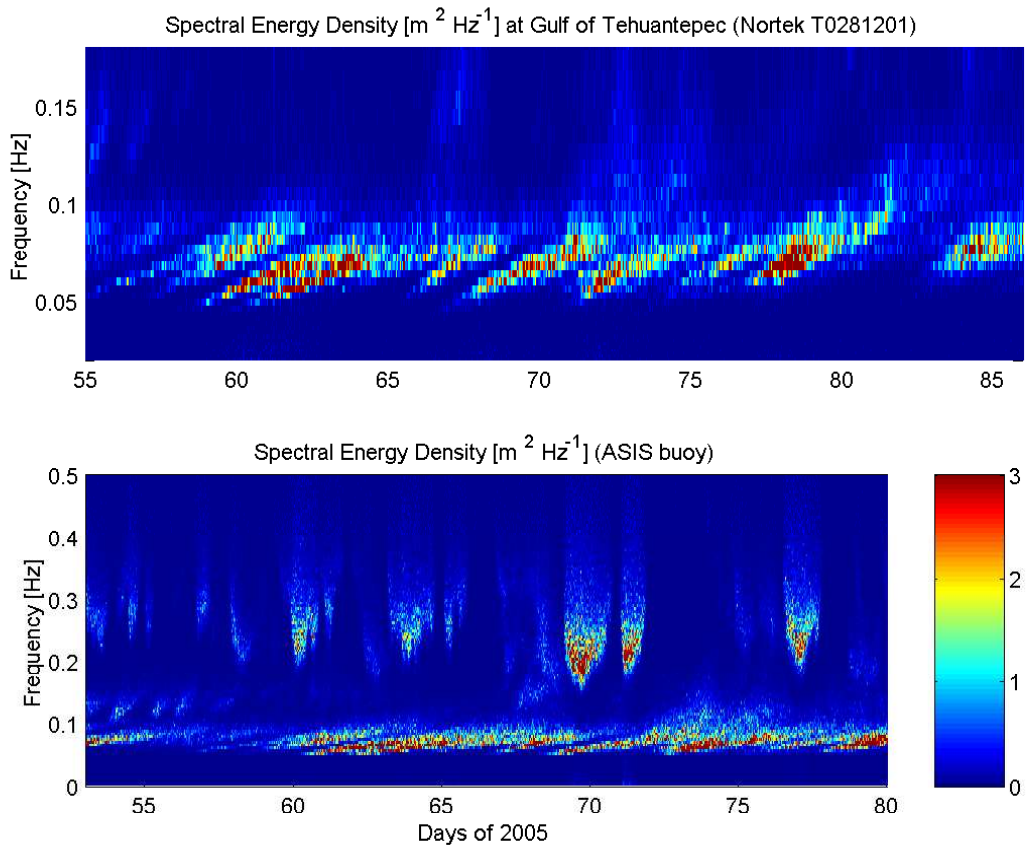


**Figure 7.** Time series of wave spectra as a function of frequency obtained from a) ADCP measurements nearshore at Castillo Station (water depth is 20 m approximately), and b) ASIS buoy (water depth about 60 m). Note the different scales, both in frequency and time, in order to better appreciate spectral energy features from each type of measurements.

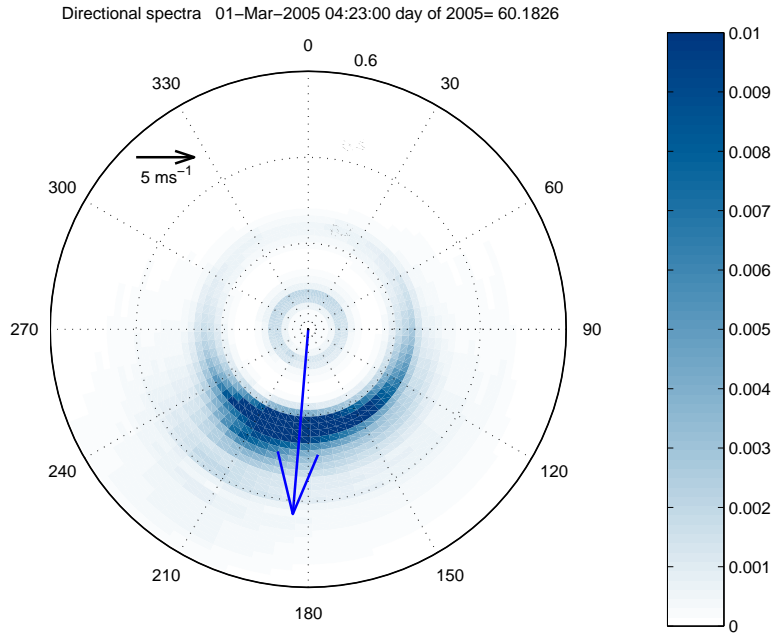


**Figure 8.** Ocean surface wave directional spectrum [ $\text{m}^2\text{Hz}^{-1}$ ] calculated from ASIS buoy measurements for a particular time when a Tehuano event was on. Direction is measured clockwise from North, while frequency is measured away from the plot origin up to a maximum of 0.6Hz. Loci for 0.2Hz and 0.4Hz are indicated (dotted circles). Wind speed scale is shown with an horizontal arrow equivalent to  $5\text{ms}^{-1}$ .

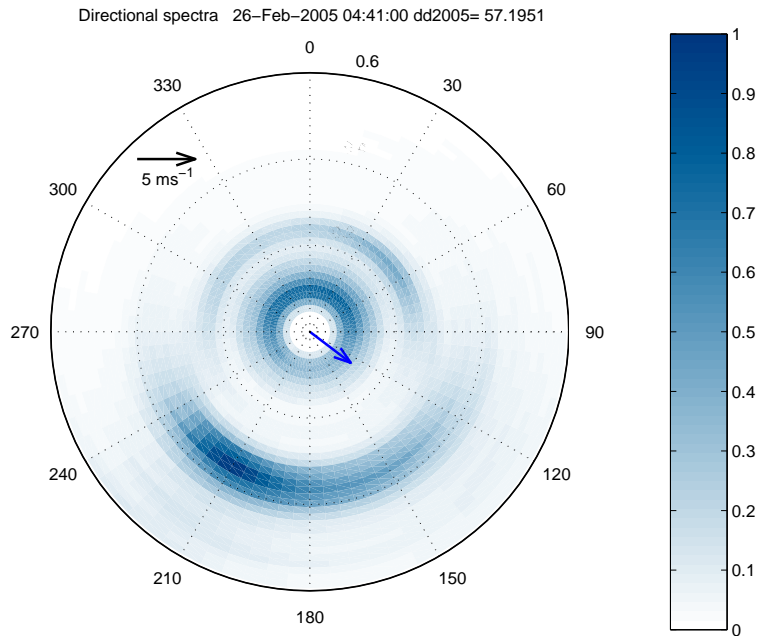


**Figure 9.** Ocean surface wave directional spectrum similar to Figure 8, but for a particular time when three wave systems were present. Note that spectral energy density scale is 0 to  $1 \times 10^{-3} \text{m}^2\text{Hz}^{-1}$ .

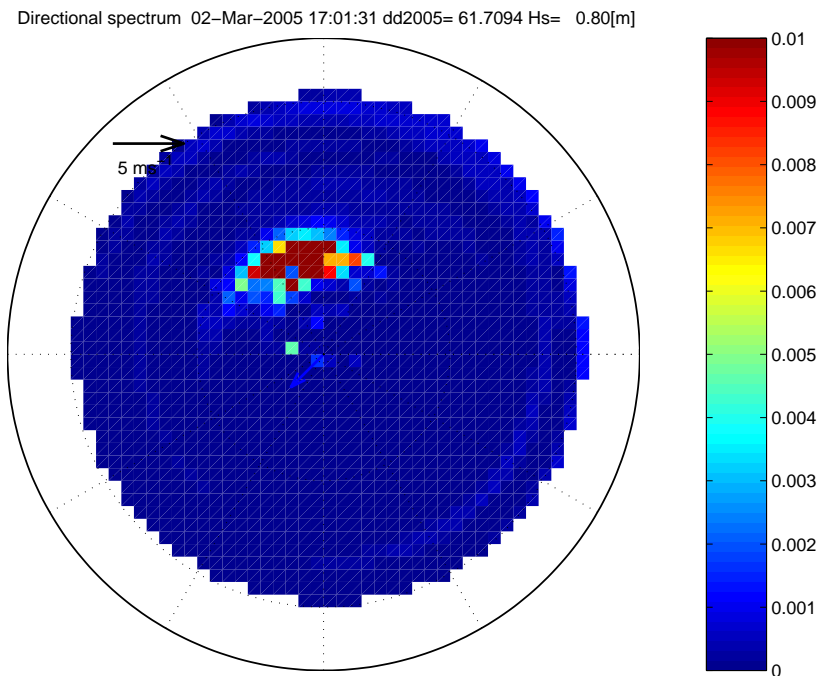


**Figure 10.** Swell directional spectrum calculated from ADCP measurements nearshore at Chipegua station, for a particular time (March 02, 2005 at 17:01 h) very close to one ASAR image acquisition for the study area. Maximum frequency is 0.25 Hz, and loci for 0.1Hz and 0.2Hz are indicated (dotted circles). Note that spectral energy density scale is 0 to  $1 \times 10^{-2} \text{ [m}^2\text{Hz}^{-1}\text{]}$ .

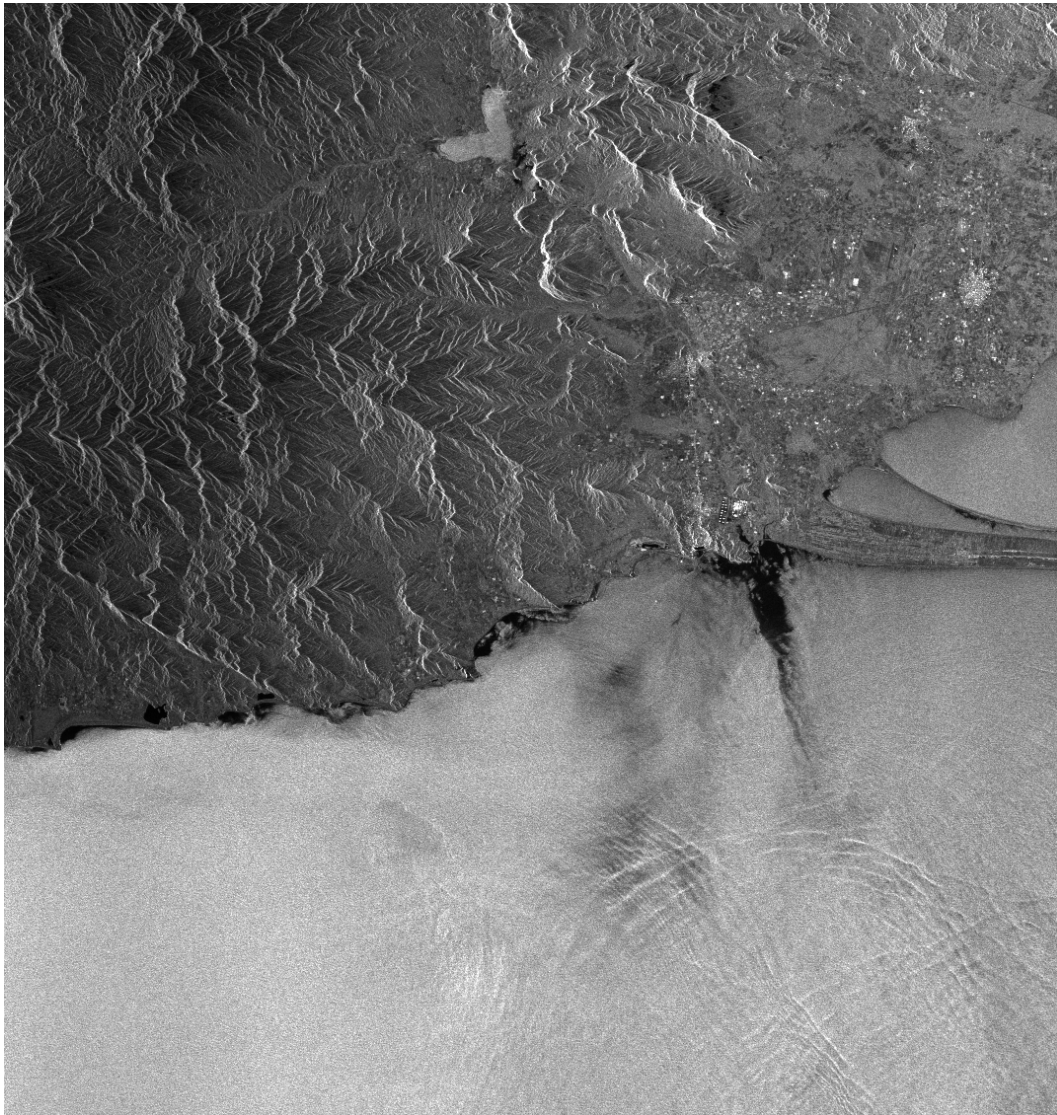


**Figure 11.** ASAR image of the Gulf of Tehuantepec acquired during the INTOA experiment in 2005.

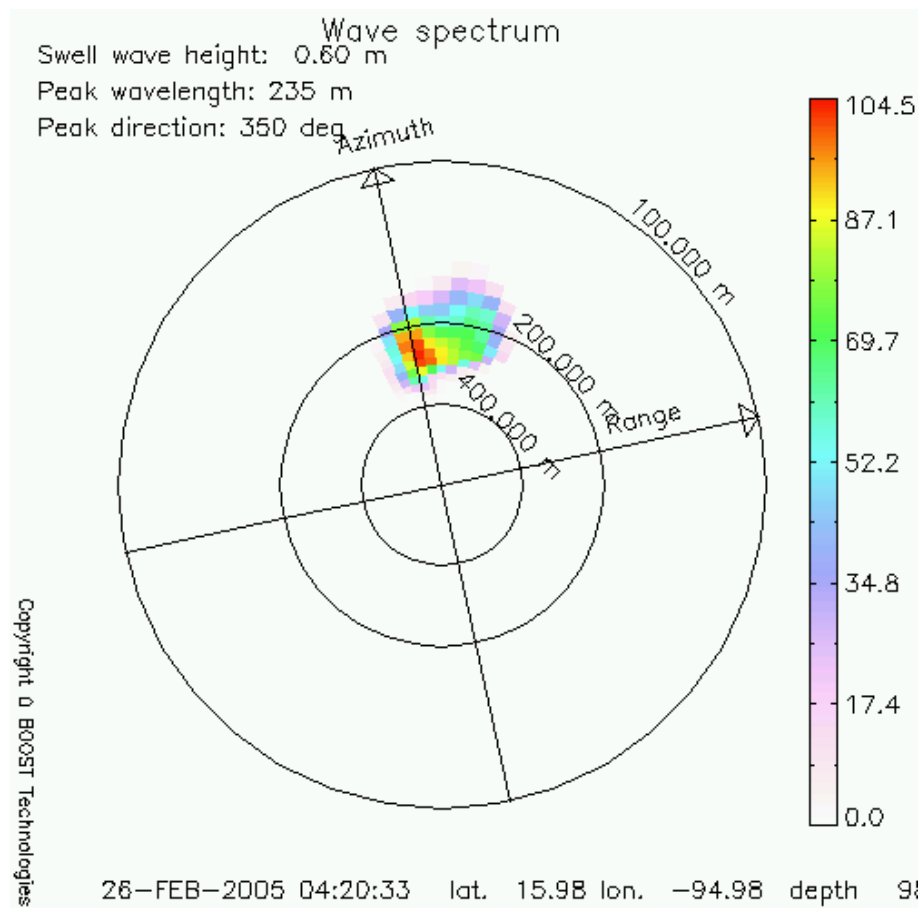


**Figure 12.** Directional wave spectrum as obtained through the inversion of the ASAR sub-image spectrum from location centered at 15.98°N and 94.98°W.

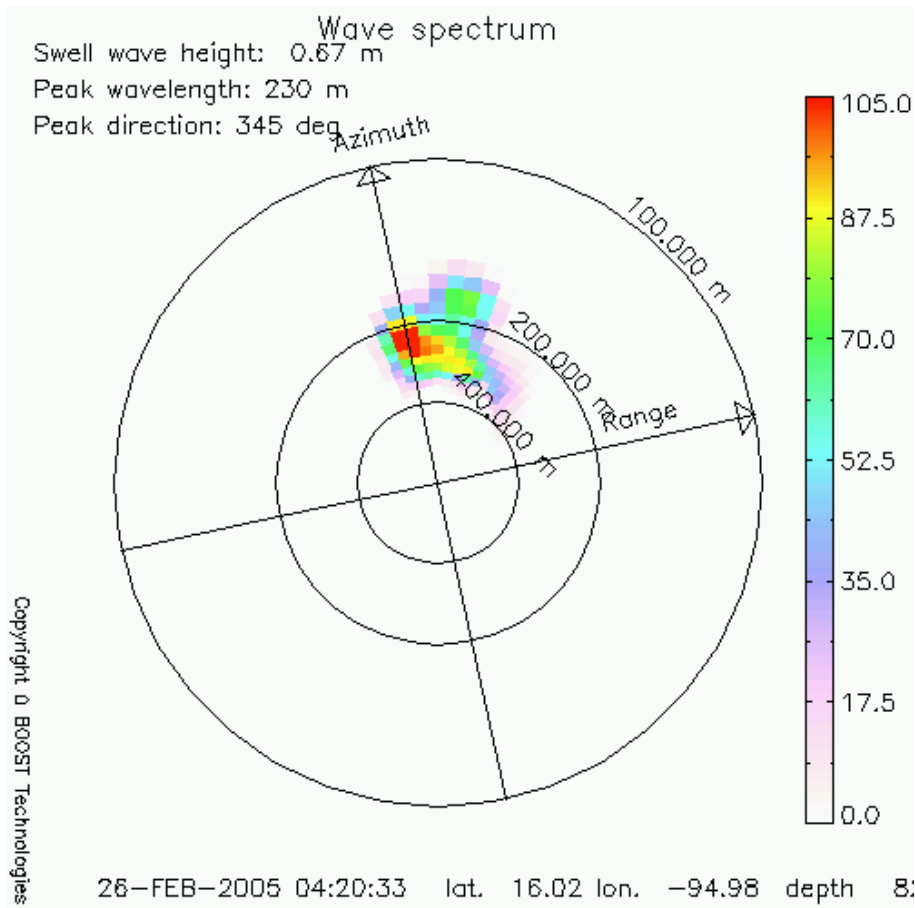


**Figure 13.** Directional wave spectrum similar to Fig. 12, but for ASAR sub-image from location centered at 16.02°N and 94.98°W.

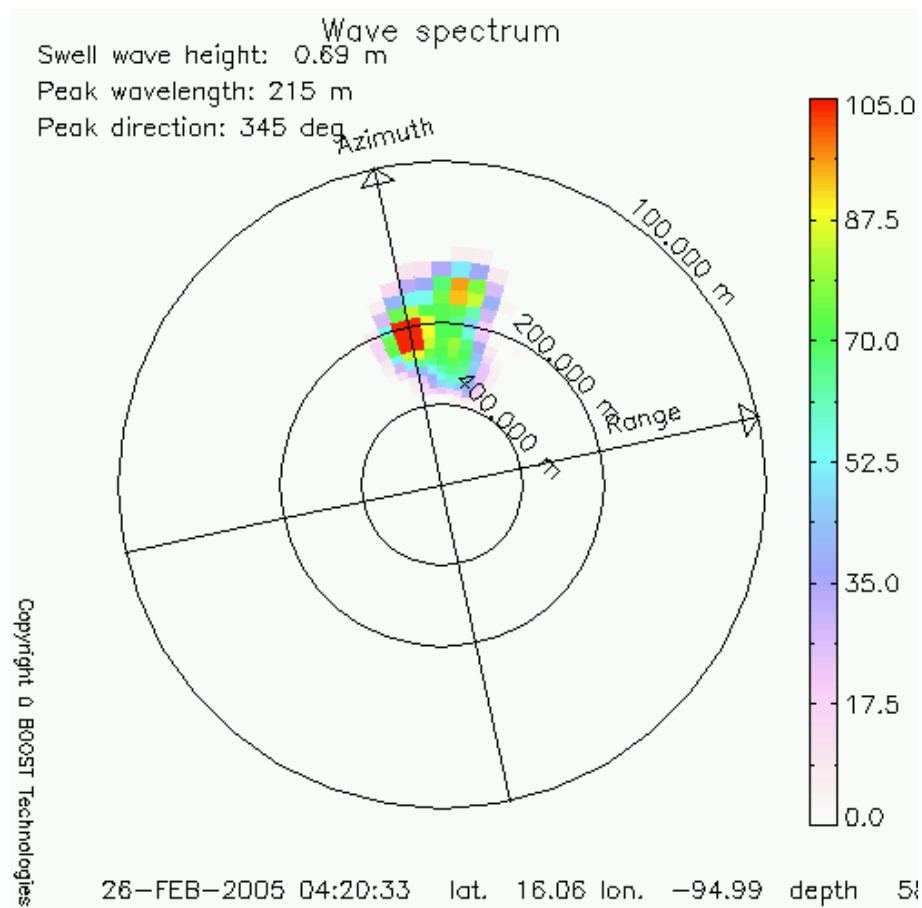


**Figure 14.** Directional wave spectrum similar to Fig. 12, but for ASAR sub-image from location centered at 16.06°N and 94.99°W.

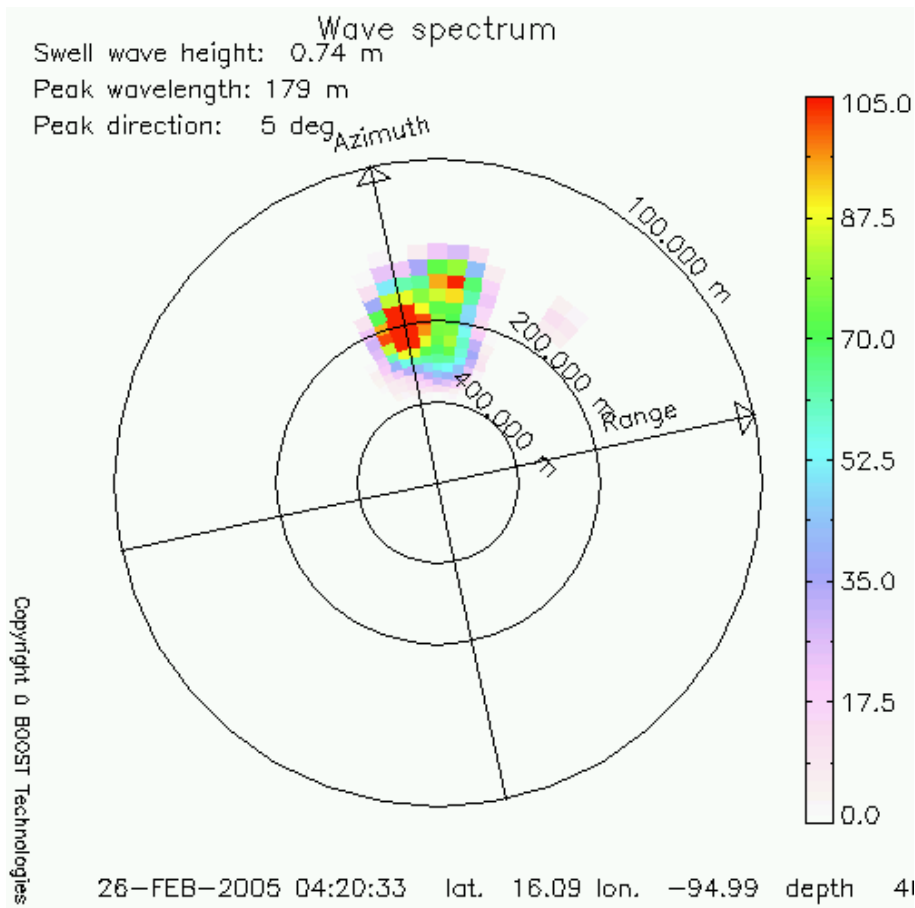


**Figure 15.** Directional wave spectrum similar to Fig. 12, but for ASAR sub-image from location centered at 16.09°N and 94.99°W.

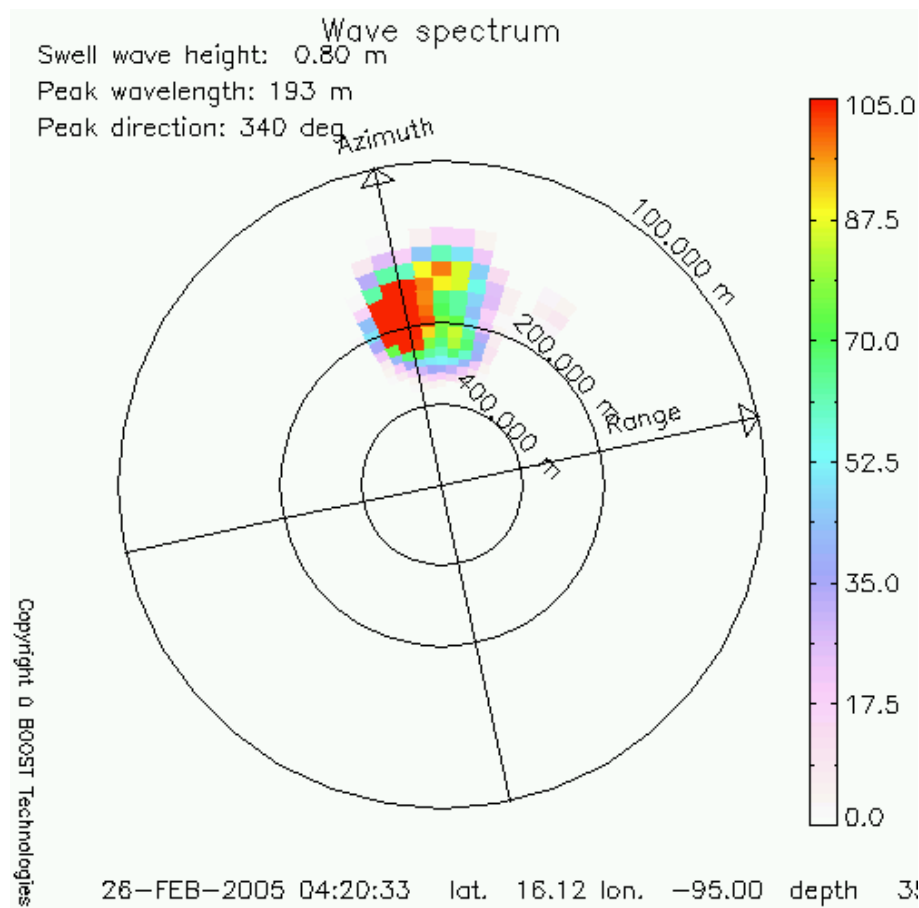


**Figure 16.** Directional wave spectrum similar to Fig. 12, but for ASAR sub-image from location centered at 16.12°N and 95.00°W.

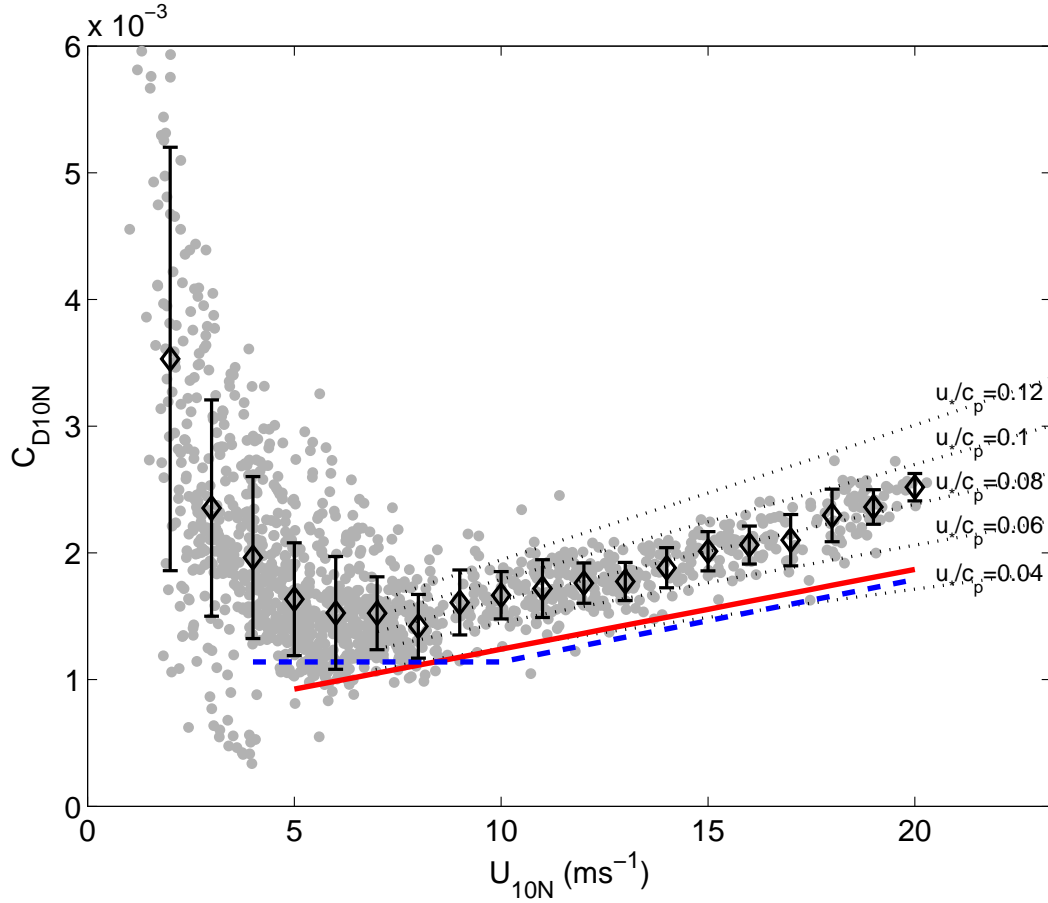


**Figure 17.** Drag coefficient from observations in the Gulf of Tehuantepec as a function of neutral wind speed. Dots represent data values for each 30 minutes, diamonds are the average  $C_{D10N}$  within wind speed bins of  $1 \text{ ms}^{-1}$  and the error bars are one standard deviation of  $C_{D10N}$  within each wind speed bin. The lines represents expected  $C_{D10N}$  from commonly used bulk formulae: 26 [26] (solid) and 20 [20] (dashed); and from constant wave age values using 12 [12] formula for pure wind seas.

**Table 1.** List of sensors and some of their characteristics used onboard the ASIS buoy for the INTOA field campaign in the Gulf of Tehuantepec during the first part of 2005

Sensor	Brand	Model	Sampling frequency	Height [m]
Sonic Anemometer	Gill	R3A	20 Hz	6.5
Capacitance Wave Gauges	CCIW		20 Hz	$\pm 1.25$
Lineal Accelerometer	Columbia Res. Lab.	SA-307HPTX	20 Hz	-7
Clinometers	Systron Donner In. Div.	GC1-00050-100	20 Hz	-7
Compass	Precision Navigation Inc.	TCM-2	1 Hz	-7
Temperature and Humidity Sensor	Jautering Int. Corp.	MP101A	1 Hz	4.5
Barometer	Setra	270	1 Hz	2.5
Thermograph	Richard Brancker Res.	TR-1050P	0.2 Hz	2.5
Currentmeter	General Oceanics Inc.	UCM-600L	5 Cyc $\text{hr}^{-1}$	-6

**Table 2.** Characteristics of Tehuano events occurred during the INTOA field campaign in the Gulf of Tehuantepec in early 2005

Label for Event	Start date and time (GMT)	Duration [h]	Mean Speed [ $\text{ms}^{-1}$ ]	Maximum Speed [ $\text{ms}^{-1}$ ]
TE1	22 Feb 2005 01:04	87	8.45	12.33
TE2	25 Feb 2005 08:54	50	5.89	10.79
TE3	28 Feb 2005 05:59	117	8.84	15.96
TE4	02 Mar 2005 23:53	137	9.53	13.57
TE5	09 Mar 2005 00:17	140	12.91	19.26
TE6	16 Mar 2005 09:55	66	11.61	15.89
TE7	22 Mar 2005 10:13	18	5.17	8.33
TE8	26 Mar 2005 16:33	91	11.98	18.66